Tunneling of electrons between Si nanocrystals embedded in a SiO_2 matrix

K. Seino* and F. Bechstedt
Institut für Festkörpertheorie und -optik, Friedrich Schiller Universität Jena, Max-Wien-Platz 1, D-07743 Jena, Germany

P. Kroll
Department of Chemistry and Biochemistry, The University of Texas at Arlington, Arlington, Texas 76019, USA
(Received 21 December 2011; revised manuscript received 21 June 2012; published 16 August 2012)

Based on *ab initio* density functional calculations of Si nanocrystals (NCs) in a SiO_2 matrix we study the impact of NC size and separation on electronic properties and present consequences for inter-NC carrier transport. The NC size and separation significantly influence the electronic structure of three-dimensional superlattice systems with different NC filling. The energy levels for large NC distances are broadened to minibands for small separations due to the wave-function overlap. Their formation is described in terms of inter-NC hopping and carrier tunneling. We find that electron transport in conduction minibands is more likely than hole transport.

DOI: 10.1103/PhysRevB.86.075312 PACS number(s): 73.22.−f, 73.63.Kv, 78.67.Bf

I. INTRODUCTION

Silicon quantum dots (Si QDs), or silicon nanocrystals (Si NCs), have been subject of intense research for the past almost two decades. Activities were driven by fundamental scientific interests as well as by promising applications in next-generation quantum devices for energy conversion and communication technology.[1–5] The effect of quantum confinement on electrons and holes due to the reduced dimensions of Si NCs will overcome the limitations of the indirect-gap semiconductor Si for optoelectronic devices. Silicon nanostructures are also viewed to pave the road toward Si-based solar cells of the third generation.[6]

Energy conversion efficiency is the key parameter for all photovoltaic technologies. Si NCs embedded in amorphous SiO_2 have been identified to improve the conversion efficiency[7,8] as follows. (i) Quantum confinement effects allow to tailor the effective bandgap.[3,5,9,10] Multistack solar cells with varying fundamental gaps overcome the Shockley-Queisser limit of 30%. A Si-based tandem cell has a theoretical efficiency limit of 60%.[6] (ii) The conversion of high-energy photons of the solar spectrum in bulk Si is limited by carrier relaxation and hence heat generation. The stronger excitonic effects in nanostructures will allow the transformation of high-energy photons into low-energy electron-hole pairs via multiple-exciton generation or quantum-cutting processes.[4,10]

The key properties of nanoscale Si-based solar cells are related to the Si-SiO_2 interfaces and the embedding insulating matrix. The interfaces constitute energy barriers $\Delta\tilde{E}_c$ and $\Delta\tilde{E}_v$ for both carrier types, electrons, and holes, with a height of the order of several electron volts.[11–13] Carrier transport from Si dots into or through the matrix is unlikely for thick and intact dielectrics. Only charge diffusion from charged to neighboring uncharged Si NCs seems to be possible.[14] Quantum confinement in Si nanostructures, thus, generates a dilemma: The increased absorption and decreased relaxation in localized QDs[15] appears opposite to the sufficient charge extraction and transport in bulk Si (Ref. 16). Electron-hole pairs photoexcited in a device have to be separated into free electrons and free holes, which in turn will travel to their respective negative and positive electrodes. The fundamental problem then is how to exploit the favorable optical properties of Si NCs, while at the same time increasing the mobility and transport of carriers in the device. Clearly, any solution to this predicament demands to understand the principle transport mechanisms in the device (e.g., miniband transport or hopping).[17,18]

In this paper we provide a detailed insight into the problem by investigating the behavior of the most relevant electronic states in Si NC arrangements and their impact on inter-NC carrier transport. We focus on the highest occupied and lowest empty NC electronic states and elucidate their relevance for tunneling processes, which are most fundamental here as well as in many fields of physics.[19] In particular, we study the interactions between electronic states localized nominally in different NCs and their dependence on the separation between the NCs. We analyze our results in the context of wave-function overlap, miniband transport, and NC hopping.

II. *AB INITIO* DESCRIPTION

A. Superlattice systems

As model systems we investigate three-dimensional arrangements of nearly spherical Si NCs of diameter D in a simple cubic (sc) lattice with lattice constant A and a single NC per unit cell. The space between the NCs is filled with an amorphous SiO_2 matrix. The minimum distances $B = A - D$ between surfaces of neighboring NCs occur in the $\langle 100 \rangle$ directions. For appropriate D and A values such arrangements combine properties of individual NCs and collective properties of the arrays and, hence, represent NC solids. Such systems have been experimentally realized[2,3,7,20] applying a method of Zacharias *et al.*[21] to photovoltaics, though their NC arrangement is closer to an orthorhombic than a simple cubic lattice. The size of the NCs and their density and, hence, the filling factor f are tunable. An illustration of a simple-cubic cell with a Si NC and embedding SiO_2 is displayed in Fig. 1. Such superlattice arrangements, of course, describe idealized systems of NC arrangements. In real samples these arrangements are influenced by two different types of disorder. (i) First, there is a size distribution of the NCs. It is accompanied by different characteristic energy levels

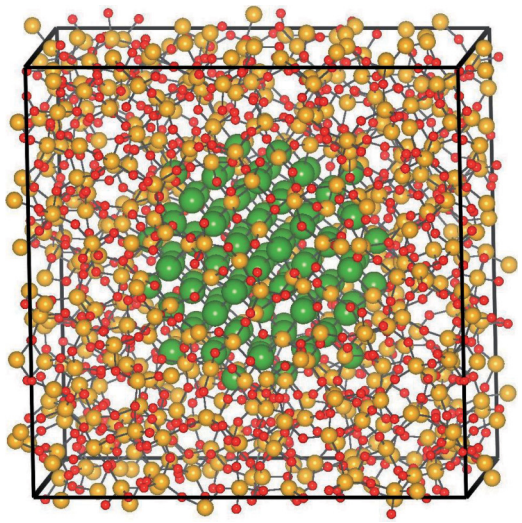

FIG. 1. (Color online) Three-dimensional representation of a cubic unit cell (black solid lines) with a Si NC illustrated by Si core atoms (large green circles) and the SiO_2 barrier material with Si and O atoms as dark red and bright yellow dots, respectively. The nominal diameter of $D = 1.6$ nm and lattice constant of $A = 2.6$ nm correspond to 99 Si core atoms and 1189 matrix atoms.

in the NCs due to varying confinement. Together with the high-energy barriers due to the surrounding oxide, this (diagonal) disorder in the site energies implies that electrons and holes may experience Anderson localization.[22] Therefore, for efficient charge transport the fluctuations of the site energies should be small. Hopping transport becomes dominant at large disorder.[23,24] (ii) There is a second kind of disorder related to fluctuating distances between NCs. The principal effect of this (off-diagonal) disorder will be discussed below by varying the superlattice constant. One expects that only NCs in a small distance contribute to the transport of carriers which will take the most efficient paths. However, recent experiments[25] showed that the carrier mobility is independent of size disorder, indicating further open questions for transport in NC solids. Also recent transport simulations within the kinetic Monte Carlo framework demonstrate only a weak reduction of carrier mobility by disorder at room temperature.[26]

The use of such Si nanodot superlattices as in Fig. 1 with a certain barrier material is in complete agreement with a general modeling of nanostructures by means of periodic boundary conditions with the resulting Bloch character of the electronic eigenstates. Similar simple-cubic arrangements have been studied for cubic Si quantum dots together with the effective-mass approximation (EMA), bulk effective electron masses, and model parameters for the energy barriers between Si, SiC, SiO_2, and Si_3N_4 (Refs. 27 and 28). However, there are several theoretical[29] and experimental[30] indications that the effective-mass concept is simply not valid in nanostructured systems, or at least, size-dependent effective masses have to be taken into account. First-principles methods are parameter free and do not need questionable approximations as the EMA for small NCs or input from experiment. The mutual influence of neighboring NCs and the effect of tunneling processes for varying NC distance is demonstrated by varying the lattice constant A and the NC size D. Also the limiting cases of isolated but embedded and strongly interacting NCs can be studied.

B. Electronic structures

The calculations are based on the density functional theory (DFT)[31] within the local density approximation (LDA) for the exchange-correlation functional[32] and explicitly performed using the Vienna *Ab initio* Simulation Package (VASP) implementation.[33] The electron-ion interaction is described within the projector augmented-wave (PAW) method.[34] The electronic eigenstates are expanded into plane waves until a cutoff energy of 400 eV. The Brillouin-zone (BZ) integrations are carried out using only the Γ point. The Kohn-Sham eigenstates and eigenvalues[32] are used to describe the electronic structure of the superlattice system. Since the quasiparticle excitation aspect is missing, the resulting energy differences between occupied and empty states are underestimated.[35] For instance, the calculated fundamental gap values for bulk Si and SiO_2 (ideal β cristobalite) are 0.44 and 5.26 eV. Nevertheless, the DFT-LDA gives a reasonable band dispersion[35] which is most important for transport description.[36] Also the band offsets are reasonably described.[12] This especially holds for their reduction due to the confinement in the NC cores which has been experimentally confirmed.[37]

To describe the correct absolute positions of the energy levels quasiparticle (QP) corrections of the Kohn-Sham eigenvalues were recently also taken into account for Si nanocrystals.[38,39] Thereby, the exchange-correlation (XC) self-energy is approximated in the framework of Hedin's GW approximation with the single-particle Green's function G and the screened Coulomb potential W.[40] The corrections give rise to shifts of occupied (empty) states toward lower (higher) energies and, hence, open the energy gaps. Recently, it has been shown that a certain amount of the QP effects can be also simulated by replacing the semilocal XC potential in the Kohn-Sham equation by a nonlocal one derived from a hybrid XC functional.[11,41] For the illustration of the QP effects on the energy positions in Fig. 2 for the density of states (DOS) we use the hybrid functional of Heyd, Scuseria, and Ernzerhof (HSE).[42] The main effect of the QP corrections results in the above-discussed shifts toward lower and higher energies. We distinguish Si atoms in the core, the interface, and the matrix according to the number of neighboring O atoms 0, 1–3, or 4.[43] In the Si NC core and the interface regions, especially in the energy region of the fundamental gap, the DOS lineshape remains unaffected, only the empty states are more or less rigidly shifted to higher energies by about 0.7 eV. This indicates that the band dispersion near the band edges is less influenced, so that the LDA results can be indeed used to investigate charge-carrier transport. The projected DOS onto the Si atoms in the SiO_2 matrix also show a shift toward lower energies by 0.6 eV of occupied states besides the 1.5 eV shift toward higher energies of the conduction states. The second group of energy shifts can be interpreted as the increase of the band discontinuities $\Delta\tilde{E}_{c/v}$ between Si NCs and SiO_2 matrix material due to the inclusion of the excitation effect.[11] These barrier increases indicate that the LDA results discussed throughout this paper may somewhat overestimate the transport between NCs through the matrix.

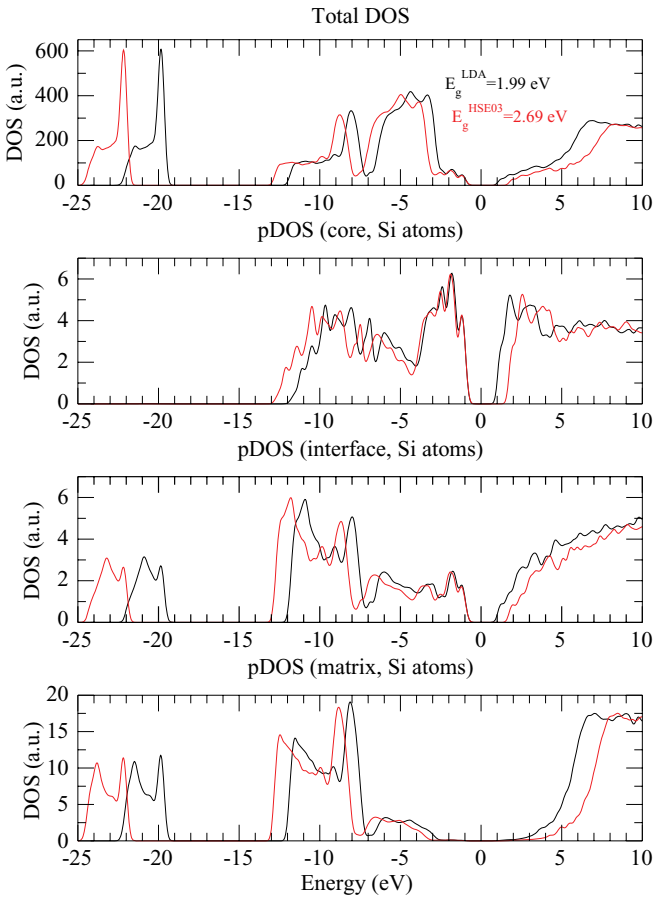

FIG. 2. (Color online) Density of states (DOS) of Si NCs with a nominal diameter $D = 1.2$ nm and lattice constant $A = 1.9$ nm within two approximations for the exchange and correlation functional, LDA (dark black line) and HSE03 (bright red line). In addition, the DOS projected onto the Si atoms in three regions, Si NC core, Si/SiO_2 interface, and SiO_2, are plotted.

C. NC construction

The construction of optimized supercell geometries for the Si NCs embedded in amorphous SiO_2 has been described in detail in Refs. 43 and 44. We use a five step procedure. At first, Si diamond supercells $2 \times 2 \times 2$, $3 \times 3 \times 3$, and $4 \times 4 \times 4$ with edge lengths between 1.1 and 2.6 nm are taken as starting geometries. They nominally contain 64, 216, and 512 Si atoms. In a supercell an almost spherical Si NC with 29, 47, 71, or 99 atoms (i.e., with a nominal diameter of $D = 1.0$, 1.2, 1.4, and 1.6 nm) is chosen. In the remaining part of the supercell O atoms are inserted into the Si–Si bonds within the third step. A bond-switching algorithm together with a randomizing procedure leads to an amorphous SiO_2 network. In the last step, a local network relaxation by means of the *ab initio* DFT optimization is used to make the bonding topology stress-free. The atomic geometries are considered to be in equilibrium when the Hellmann-Feynman forces are smaller than 10 meV/Å. By construction, Si–O–Si bridge bonds form the interface, once B approaches 0.2 nm or larger values. Optimized geometries with interface defects (e.g., dangling bonds) are not further investigated. The resulting structures are characterized in Table I by the geometry parameters D and B, the numbers of Si NC atoms N_{NC}, and the total number of atoms N_{total} in a supercell. In addition, the systems are described by the filling factor f which is the ratio of NC volume and total cell volume. The filling factors f vary in the range of 0.06–0.65.

The majority of the systems in Table I possesses a sufficiently thick minimum thickness $B \geqslant 0.5$ nm in the cubic-axis directions ⟨100⟩ to speak about NCs and matrix material in-between. However, in the other three models with $B \leqslant 0.2$ nm the barriers are small in the Cartesian directions. However, even for $B = 0.0$ nm the barrier thickness is finite in other directions [e.g., in a body-diagonal direction it amounts to $(\sqrt{3} - 1)A = 0.9$ nm]. Indeed, these models exhibit bond percolation,[12,44] effectively a few intercluster Si–Si bonds. This most extreme situation is displayed in Fig. 3. This $Si_{47}(2 \times 2 \times 2)$ arrangement possesses a maximum of Si–Si bonds between neighboring clusters. We observe eight such intercluster bonds from a total number of 12 for two adjacent NCs in a Cartesian direction. Electrons (or holes) may be transported along these Si–Si bond paths without scattering by oxygen atoms. The impact of such intercluster Si–Si bond paths on carrier transport is discussed below in terms of the miniband dispersion.

III. ELECTRONIC STRUCTURE AND TRANSPORT

A. Minibands, hopping integrals, and carrier masses

For the eight systems of three-dimensional Si NC arrangements embedded in amorphous SiO_2 and characterized in

TABLE I. Models studied for embedded Si NCs with number of Si NC atoms N_{NC}, total number of atoms in the supercell N_{total}, nominal NC diameter D, separation between neighboring NCs B, and filling factor f. In addition, resulting bandgaps E_g and inter-NC hopping integrals t for the Γ-X (Γ-M) direction are listed.

Model	N_{NC}	N_{total}	D (nm)	B (nm)	f	E_g (eV)	t (meV)
$Si_{29}(2 \times 2 \times 2)$	29	116	1.0	0.2	0.28	1.60	20 (4)
$Si_{29}(3 \times 3 \times 3)$	29	572	1.0	1.0	0.06	2.23	0 (0)
$Si_{47}(2 \times 2 \times 2)$	47	80	1.2	0.0	0.65	0.73	56 (65)
$Si_{47}(3 \times 3 \times 3)$	47	524	1.2	0.7	0.12	1.99	0 (1)
$Si_{71}(3 \times 3 \times 3)$	71	464	1.4	0.5	0.21	1.71	3 (2)
$Si_{71}(4 \times 4 \times 4)$	71	1352	1.4	1.2	0.08	1.90	0 (0)
$Si_{99}(3 \times 3 \times 3)$	99	400	1.6	0.2	0.37	0.50	58 (51)
$Si_{99}(4 \times 4 \times 4)$	99	1288	1.6	1.0	0.12	1.76	0 (0)

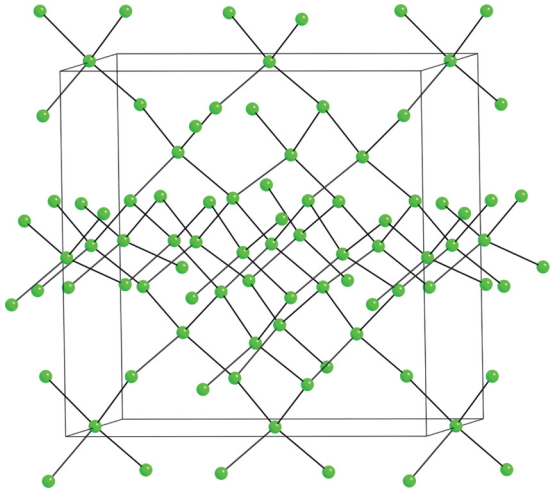

FIG. 3. (Color online) Bonds between Si atoms (green dots) for the $Si_{47}(2 \times 2 \times 2)$ model with $D = 1.2$ nm and $B = 0.0$ nm. The unit cell is indicated by solid lines.

Table I we have calculated the electronic band structures versus high-symmetry lines in the BZ of the corresponding sc crystals. For two classes of NCs with 47 ($D = 1.2$ nm) and 99 ($D = 1.6$ nm) Si core atoms but different lattice constant A the atomic arrangements are depicted in Fig. 4 together with the resulting band structures. The differences between well-isolated and interacting NCs are clearly visible. The noninteracting NCs in Figs. 4(b) and 4(d) give rise to flat bands around the fundamental gap, which in turn can be identified with the energy levels of the isolated NCs.[43] The energy difference between the lowest unoccupied molecule orbital and highest occupied molecule orbital defines the (Kohn-Sham) gap E_g (Ref. 32). It is enlarged with respect to its bulk value by quantum size effects and varies remarkably with the NC diameter as $D^{-\beta}$ with $\beta \lesssim 1$ in the experiment[2] and theory.[43] Note that the presence of the SiO_2 matrix drastically reduces the gap size with respect to the case where the Si NC surface is passivated by hydrogen atoms (see Ref. 43).

Reducing the matrix material between neighboring NCs toward values $B < 0.5$ nm, especially along the cubic axes, broadens the energy levels to minibands. In particular, this is observed for unoccupied states in Figs. 4(a) and 4(c), but is also seen for occupied states in the case of almost vanishing separation B [see Fig. 4(c)]. Besides band dispersions, the fundamental gap E_g is influenced also. E_g is significantly reduced, the data are given in Table I. In the limit of small B the embedded-NC systems become indirect semiconductors. The minimum of the lowest conduction miniband (LCMB) is located at the Γ point, while the $\mathbf{k}$-space position of the maximum of the highest valence miniband (HVMB) is at the BZ boundary edge, but fluctuates between R and M. Both the reduction of the bandgap and the band dispersion depend on B. A clear energetical ordering $\varepsilon(\Gamma) < \varepsilon(R) < \varepsilon(X) < \varepsilon(M)$ of the minima and maxima of the LCMB $\varepsilon(\mathbf{k})$ at high-symmetry points is observed.

The different dispersions of the minibands have wide implications on transport properties of photoexcited electrons and holes between Si NCs.[2] This is well known from miniband transport in one-dimensional superlattices.[45] The dispersion of the highest valence miniband is weak for the models

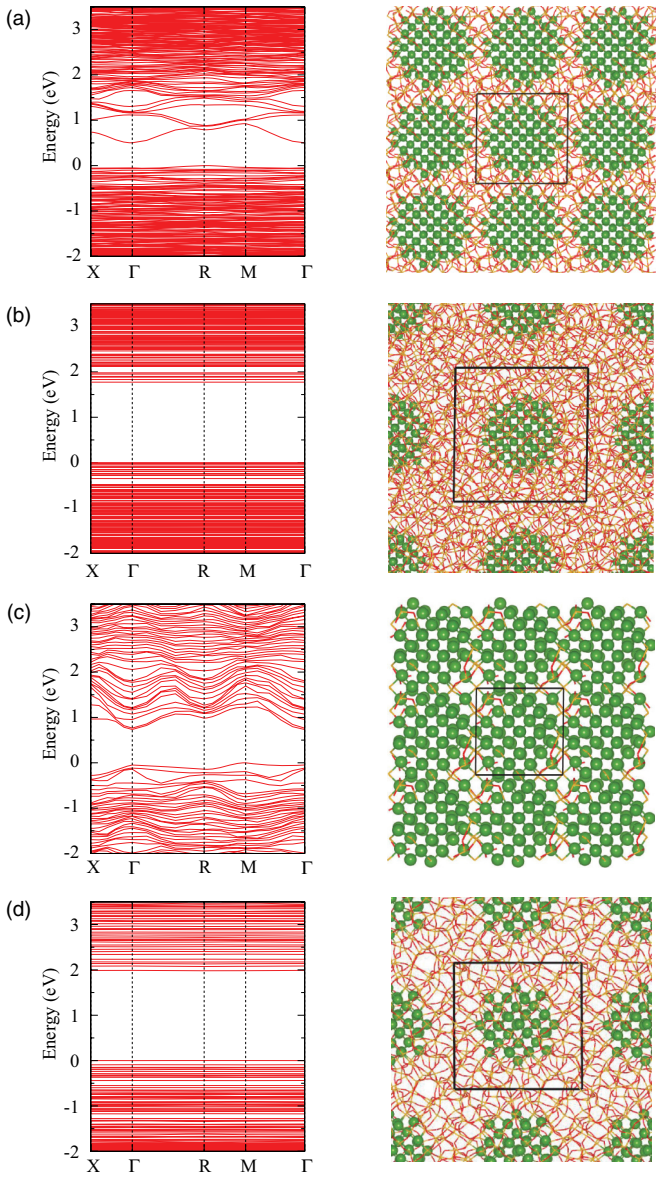

FIG. 4. (Color online) Band structures (left panels) and atomic structures (right panels) of the models (a) $Si_{99}(3 \times 3 \times 3)$, (b) $Si_{99}(4 \times 4 \times 4)$, (c) $Si_{47}(2 \times 2 \times 2,)$ and (d) $Si_{47}(3 \times 3 \times 3)$. The atomic geometries are indicated as projections onto a (001) plane. Green balls represent Si atoms in the core. The amorphous SiO_2 networks are depicted by thin red lines. The black lines indicate the unit cells with varying lattice constant (a) $A = 1.2$, (b) 1.9, (c) 1.8, and (d) 2.6 nm. The highest occupied state is used as energy zero.

$Si_{47}(2 \times 2 \times 2)$ and $Si_{99}(3 \times 3 \times 3)$ with vanishing or small B. The small band curvature at the maxima at R and M indicates large effective hole masses and, hence, less mobile holes. Focussing our discussion on the electrons in the LCMB $\varepsilon(\mathbf{k})$, we observe a strong dispersion for this band (cf. Figs. 4 and 5). The implication of the dispersion on the transport mechanism of the electrons can be interpreted in terms of miniband transport. Following the ideas developed to treat the carrier transport between large molecules in organic semiconductors (see the reviews in Refs. 36 and 46) a tight-binding approach to the LCMB leads to hopping integrals illustrating the strength for hopping from one NC site to another one. Restricting to

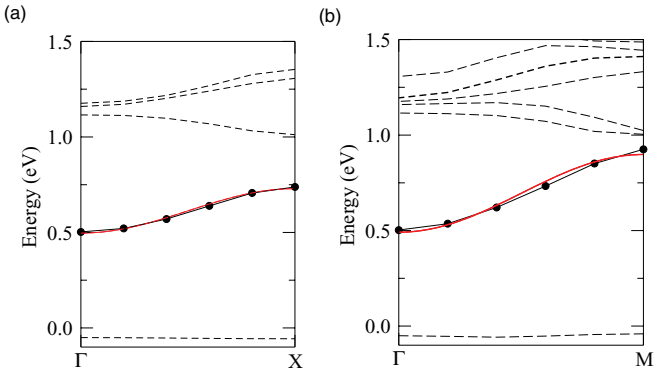

FIG. 5. (Color online) Band structure (dashed lines and dots) between Γ and X and fit curve (red, solid line) for the LCMB using Eq. (1) for the $Si_{99}(3 \times 3 \times 3)$ model. The HVMB maximum is used as energy zero.

nearest-neighbor NCs, the corresponding hopping integral t follows from a tight-binding approach as

$$\varepsilon(\mathbf{k}) = \varepsilon_0 - 2t[\cos(k_x A) + \cos(k_y A) + \cos(k_z A)], \quad (1)$$

with ε_0 as the energy of the electronic level formed for large separations between the NCs. In Fig. 5 we show an example of the fit using Eq. (1) for the model $Si_{99}(3 \times 3 \times 3)$ and the LCMB along the high-symmetry lines between Γ and X as well as Γ and M. The resulting t values for the eight three-dimensional superlattices of Si NCs embedded in SiO_2 are listed in Table I. For comparison, results obtained for both directions Γ-X and Γ-M are given. The magnitude of hopping integrals t for small separations approaches values for the corresponding hole quantities in molecular semiconductors fabricated by different organic molecules.[36] We find a strong influence of the separation between the NC surfaces, for example, with $t = 58$ or 51 meV for $B = 0.2$ nm (see Fig. 5) and $t \sim 0.0$ meV for $B = 1.0$ nm comparing the models $Si_{99}(3 \times 3 \times 3)$ and $Si_{99}(4 \times 4 \times 4)$ with fixed NC diameter. Interestingly, the hopping integrals for the systems $Si_{47}(2 \times 2 \times 2)$ and $Si_{99}(3 \times 3 \times 3)$ are rather similar despite the different intercluster spacings $B = 0.0$ and 0.2 nm. The hopping integrals t for systems with significant miniband dispersion give an upper limit for the diagonal disorder[22,23] for which miniband transport is still possible. With $t \approx$ 50 meV (see Table I) and a thickness variation $\sim D^{-0.5}$ of the confinement energies[43] only small diameter fluctuations of a few percent are allowed.

The tight-binding approach Eq. (1) can be directly related to the effective mass of electrons in the LCMB of the NC arrangement near Γ by $m^* = \hbar^2/(2tA^2)$. From the fitting shown in Fig. 5 we obtain $m^* = 0.20m$, a value comparable to the smallest conduction band mass of bulk silicon.[47] Since the carrier mobility μ due to miniband conduction is proportional to the inverse effective mass, one finds

$$\mu \sim \frac{1}{m^*} \sim tA^2, \quad (2)$$

in qualitative agreement with expressions for coherent transport in superlattices and crystals of molecular systems.[8,36,46]

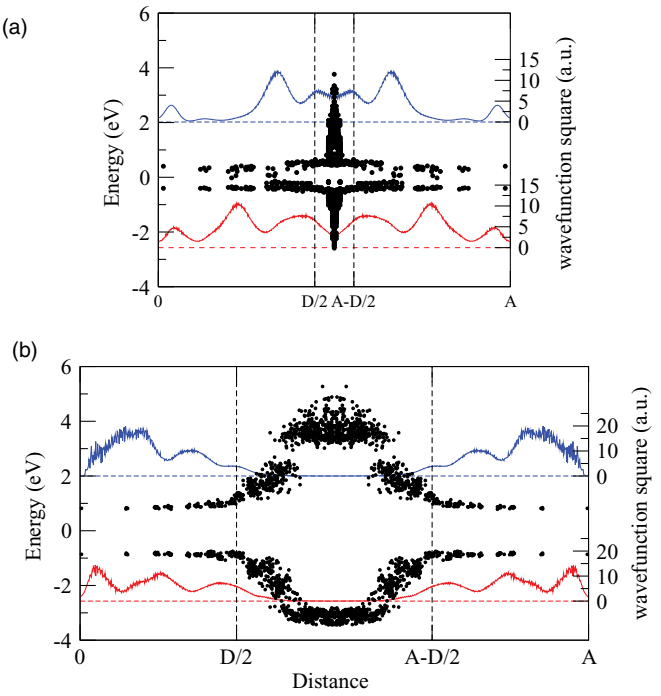

FIG. 6. (Color online) Radial probability distributions of highest valence miniband (HVMB) and lowest conduction miniband (LCMB) state as a function of the distance r from the center of a Si NC for the (a) $Si_{99}(3 \times 3 \times 3)$ and (b) $Si_{99}(4 \times 4 \times 4)$ models. The wave-function squares are averaged for each r. In addition, the energies of the local lowest conduction (E_c) and highest valence (E_v) states are depicted as dots to illustrate the respective energy barriers $\Delta\tilde{E}_c$ and $\Delta\tilde{E}_v$. The situation of two neighboring NCs in a Cartesian direction is displayed.

B. Wave-function overlap and tunneling

The magnitude of the hopping integrals in Eq. (1) depends on the overlap between electronic wave functions localized in adjacent NCs. In Fig. 6 we plot the wave-function squares (i.e., the radial probability distributions of HVMB and LCMB states as a function of the distance r from the centers of two adjacent Si NCs for two different models with equal NC diameter but different NC separation). For comparison, we also depict the local energies E_c (E_v) of the lowest unoccupied (highest occupied) levels in the region of Si NCs and SiO_2 matrix as calculated by a projection technique[12] which indicate the potential barriers for electrons (holes). Apparently, the potential barriers, especially their width, in Fig. 6(a) are smaller in comparison to that indicated in Fig. 6(b) for a system with larger separation between the NCs. In Fig. 6(a), the barrier thickness approaches the extent of the Si/SiO_2 interface.[12] In agreement with the magnitude of the hopping integrals significant overlap of the wave functions localized in different NCs only occurs for small separations ($B =$ 0.2 nm) between the NC surfaces [Fig. 6(a)]. Vanishing overlap of the wave functions occurs for a large barrier thickness ($B = 1.0$ nm) [Fig. 6(b)]. We conclude that the substantial tunneling of corresponding carriers through the respective barriers happens for small NC distances. Based on our analysis, we expect this effect to be larger for electrons, while for

holes tunneling may occur only when NCs already connect to each other [see Fig. 6(a) for $B = 0.0$ nm]. Our thickness predictions are in agreement with plausible parameters derived from measurements. Conductance measurements indicate a tolerance parameter of about 0.73 nm[48] while tunneling is known to typically occur for separations below 1.2 nm (see Fig. 4 in Ref. 49).

The above analysis is in qualitative agreement with an alternative picture for the carrier transport. The SiO_2 matrices represent potential barriers for the (coherent) tunneling of electrons and holes through them. Incoherent phonon-assisted tunneling processes[46] are not considered. Our findings in Fig. 6 fit the textbook picture of tunneling of electrons (holes) with mass m^* through a barrier with height $\Delta\tilde{E}_c$ ($\Delta\tilde{E}_v$) (Refs. 11 and 12) and thickness B (Ref. 50),

$$\mu \sim \exp\left\{-\sqrt{\frac{8m^*}{\hbar^2}}\sqrt{\Delta\tilde{E}_{c/v}}\cdot B\right\}. \tag{3}$$

The band discontinuity $\Delta\tilde{E}_c$ ($\Delta\tilde{E}_v$) and the barrier thickness B are visible in Fig. 6. The mass dependence of the mobility is the dominant factor governing the variation of μ for electrons and holes. Qualitatively the mobility expression Eq. (3) gives similar dependencies on the geometry parameters as the formula in Eq. (2). Both expressions suggest a positive conclusion for the application of Si NCs to improve the efficiency of Si-based photovoltaic devices: If the distance between the surfaces of the nanoparticles as well as their diameter fluctuations are small enough, efficient electron transport is likely. Another precondition is that the effect of the Coulomb charging energies on the carrier transfer probability is negligible.[18,26] The condition of small barrier distances (or lower barrier heights) is in agreement with experimental findings for vertical transport through Si/SiO_2 superlattices.[51] The strong influence of the barrier height $\Delta\tilde{E}_{c/v}$ has been demonstrated experimentally by the change of the matrix material. The replacement of SiO_2 by Si_3N_4 leads to their reduction to about 50% and an increase of the current by a factor 4–5 for a given voltage.[13]

Temperature- and electric-field-dependent studies of charge-carrier transport in multilayer structures of Si NCs embedded in SiO_2 established that the transport is best described by a combination of phonon-assisted and direct tunneling mechanisms.[52] However, for low electric fields tunneling is favorable in agreement with our assumption. The tunneling contribution is in qualitative agreement with the mechanism predicted in Eq. (3). Phonon-assisted processes do not occur in this approach. According to the investigations of phonon-assisted processes in molecule crystals,[53] intermolecule vibrations should dominate these processes. In analogy, inter-NC vibrations may also influence the transport between small nanocrystals as long as their atomic weights are not too large. However, until now such vibrations have not been studied. The computation of the corresponding small electron-phonon coupling constants and inter-NC vibrations is a challenge for future *ab initio* studies of embedded Si NCs with less than 150 Si atoms and vanishing distances. In the limit of narrow bands and high temperatures the many-phonon processes[53] may be described by Marcus' electron-transfer theory.[54] Brus[55] applied this theory as electron transfer kinetics to Si NCs. The characteristic parameter of the theory, the polaron binding energy,[53] is approximated by the Fröhlich coupling mechanism in a SiO_2 matrix with a polaron radius of the order of the NC one. Meanwhile the strong coupling of SiO_2 phonons to carriers in Si NCs is confirmed by photoluminescence studies.[56] However, the resulting polaron energies are large compared to the thermal energy k_BT, so that the contribution of SiO_2-phonon-assisted processes remains small. The Marcus' factor in the electron transfer rate between two NCs is weighted by the square of the transmission coefficient which decays exponentially $\sim\exp(-2\beta\cdot B)$, similar to Eq. (3), with a typical tunnel lengths $\beta^{-1} = 1.1$ Å (Ref. 57) in rough agreement with the above estimations.

IV. SUMMARY AND CONCLUSION

In summary, we have studied the probability of carrier transport between Si nanocrystals embedded in amorphous SiO_2 in the dependence of nanocrystal distance and size by first-principles calculations. The studies are mainly based on electronic-structure calculations of three-dimensional arrangements of Si nanocrystals with varying size and distance. For the case of small NC separation below 0.2 nm, we found the formation of minibands and a remarkable band dispersion especially in the conduction-band region and hence evidence of electron transport in the lowest conduction miniband. The band dispersion results in an effective mass of the charge carriers in the solid formed by nanocrystals and embedding matrix. To relate the electronic-structure results to carrier transport between NCs, we follow ideas developed for large organic molecules in semiconducting molecule crystals. Interestingly, the miniband dispersion can directly be related to hopping integrals between different Si NCs embedded in a-SiO_2. Our model provides a band-structure-based unified picture of miniband and hopping transport of electrons between adjacent NCs, at least for the coherent contribution. The incoherent contributions to the carrier mobility due to phonons are not taken into account. Because of the large atomic mass of the NCs the inter-NC vibrations possess small frequencies and coupling constants to the electrons. However, also assistance of the tunneling by barrier phonons seems to be not efficient enough. Finally, we have shown that finite miniband dispersion is directly related to the overlap of the corresponding wave functions. The carrier transport related to this effect can be also due to coherent tunneling through energy barriers.

ACKNOWLEDGMENTS

F.B. acknowledges interesting discussions with R. Müller. This work was supported by the BMBF, Germany (Projects No. 03SF0352D and No. 13N9669). P.K. is supported by the NSF (DMR-0907117). Grants of computer time from John von Neumann Institute for Computing (NIC) in Jülich, from UTA-HPC, and from the Texas Advanced Computing Center (TACC) in Austin, TX, are gratefully acknowledged.

*seino@ifto.physik.uni-jena.de

[1] L. Pavesi, L. Dal Negro, C. Mazzoleni, G. Franzo, and F. Priolo, Nature (London) **408**, 440 (2000).

[2] J. Heitmann, F. Müller, L. Yi, M. Zacharias, D. Kovalev, and F. Eichhorn, Phys. Rev. B **69**, 195309 (2004).

[3] S. Godefroo, M. Hayne, M. Jivanescu, A. Stesmans, M. Zacharias, O. I. Lebedev, G. Van Tendeloo, and V. V. Moshchalkov, Nat. Nano **3**, 174 (2008).

[4] D. Timmerman, I. Izeddin, P. Stallinga, I. Yassievich, and T. Gregorkiewicz, Nat. Photon **2**, 105 (2008).

[5] W. D. A. M. de Boer, D. Timmerman, K. Dohnalova, I. Yassievich, H. Zhang, W. Buma, and T. Gregorkiewicz, Nat. Nano **5**, 878 (2010).

[6] M. Green, *Third Generation Photovoltaics: Advanced, Solar Energy, Conversion* (Springer, Berlin, 2003).

[7] G. Conibeer, M. Green, R. Corkish, Y. Cho, E.-C. Cho, C.-W. Jiang, T. Fangsuwannarak, E. Pink, Y. Huang, T. Puzzer, T. Trupke, B. Richards, A. Shalav, and K.-L. Lin, Thin Solid Films **511-512**, 654 (2006).

[8] J.-W. Luo, P. Stradins, and A. Zunger, Energy Environ. Sci. **4**, 2546 (2011).

[9] D. Kovalev, Nat. Nano **5**, 827 (2010).

[10] M. C. Beard, K. P. Knutsen, P. Yu, J. M. Luther, Q. Song, W. K. Metzger, R. J. Ellingson, and A. J. Nozik, Nano Lett. **7**, 2506 (2007).

[11] A. Alkauskas, P. Broqvist, F. Devynck, and A. Pasquarello, Phys. Rev. Lett. **101**, 106802 (2008).

[12] K. Seino, F. Bechstedt, and P. Kroll, Phys. Rev. B **82**, 085320 (2010).

[13] D. Di, H. Xu, I. Perez-Wurfl, M. A. Green, and G. Conibeer, Progress in Photovoltaics: Research and Applications (2011), doi: 10.1002/pip.1230.

[14] C. Y. Ng, T. P. Chen, H. W. Lau, Y. Liu, M. S. Tse, O. K. Tan, and V. S. W. Lim, Appl. Phys. Lett. **85**, 2941 (2004).

[15] A. Gali, M. Voros, D. Rocca, G. T. Zimanyi, and G. Galli, Nano Lett. **9**, 3780 (2009).

[16] S.-K. Kim, C.-H. Cho, B.-H. Kim, S.-J. Park, and J. W. Lee, Appl. Phys. Lett. **95**, 143120 (2009).

[17] S. V. Goupalov, Phys. Rev. B **79**, 233305 (2009).

[18] D. V. Talapin, J.-S. Lee, M. V. Kovalenko, and E. V. Shevchenko, Chem. Rev. **110**, 389 (2010).

[19] M. Di Ventra, Nature Nanotech. **5**, 828 (2010).

[20] G. Conibeer, M. Green, E.-C. Cho, D. König, Y.-H. Cho, T. Fangsuwannarak, G. Scardera, E. Pink, Y. Huang, T. Puzzer, S. Huang, D. Song, C. Flynn, S. Park, X. Hao, and D. Mansfield, Thin Solid Films **516**, 6748 (2008).

[21] M. Zacharias, J. Heitmann, R. Scholz, U. Kahler, M. Schmidt, and J. Bläsing, Appl. Phys. Lett. **80**, 661 (2002).

[22] N. Mott, J. Non-Cryst. Solids **8–10**, 1 (1972).

[23] D. V. Talapin and C. B. Murray, Science **310**, 86 (2005).

[24] B. Skinner, T. Chen, and B. I. Shklovskii, Phys. Rev. B **85**, 205316 (2012).

[25] Y. Liu, M. Gibbs, J. Puthussery, S. Gaik, R. Ihly, H. W. Hillhouse, and M. Law, Nano Lett. **10**, 1960 (2010).

[26] H. Lepage, A. Kaminski-Cachopo, A. Poncet, and G. le Carval, J. Phys. Chem. C **116**, 10873 (2012).

[27] C.-W. Jiang and M. A. Green, J. Appl. Phys. **99**, 114902 (2006).

[28] P. Löper, R. Müller, D. Hiller, T. Barthel, E. Malguth, S. Janz, J. C. Goldschmidt, M. Hermle, and M. Zacharias, Phys. Rev. B **84**, 195317 (2011).

[29] H.-C. Weissker, J. Furthmüller, and F. Bechstedt, Phys. Rev. B **65**, 155328 (2002).

[30] E. G. Barbagiovanni, D. J. Lockwood, P. J. Simpson, and L. V. Goncharova, J. Appl. Phys. **111**, 034307 (2012).

[31] P. Hohenberg and W. Kohn, Phys. Rev. **136**, B864 (1964).

[32] W. Kohn and L. J. Sham, Phys. Rev. **140**, A1133 (1965).

[33] G. Kresse and J. Furthmüller, Comp. Mater. Sci. **6**, 15 (1996).

[34] G. Kresse and D. Joubert, Phys. Rev. B **59**, 1758 (1999).

[35] W. G. Aulbur, L. Jönsson, and J. W. Wilkins, Solid State Physics **54**, 1 (1999).

[36] F. Ortmann, F. Bechstedt, and K. Hannewald, Phys. Status Solidi B **248**, 511 (2011).

[37] G. Seguini, S. Schamm-Chardon, P. Pellegrino, and M. Perego, Appl. Phys. Lett. **99**, 082107 (2011).

[38] P. H. Hahn, W. G. Schmidt, and F. Bechstedt, Phys. Rev. B **72**, 245425 (2005).

[39] S. Ossicini, M. Amato, R. Guerra, M. Palummo, and O. Pulci, Nanoscale Res. Lett. **5**, 1637 (2010).

[40] L. Hedin, Phys. Rev. **139**, A796 (1965).

[41] F. Fuchs, J. Furthmüller, F. Bechstedt, M. Shishkin, and G. Kresse, Phys. Rev. B **76**, 115109 (2007).

[42] J. Heyd, G. E. Scuseria, and M. Ernzerhof, J. Chem. Phys. **118**, 8207 (2003).

[43] K. Seino, F. Bechstedt, and P. Kroll, Nanotechnology **20**, 135702 (2009).

[44] P. Kroll and H. J. Schulte, Phys. Status Solidi B **243**, R47 (2006).

[45] P. Yu and M. Cardona, *Fundamentals of Semiconductors* (Springer-Verlag, Berlin, 1995).

[46] F. Ortmann, F. Bechstedt, and K. Hannewald, New J. Phys. **12**, 023011 (2010).

[47] T. Ando, A. B. Fowler, and F. Stern, Rev. Mod. Phys. **54**, 437 (1982).

[48] F. Voigt, G. H. Bauer, and F. Huisken, J. Appl. Phys. **106**, 034308 (2009).

[49] J. Halbritter, G. Repphun, S. Vinzelberg, G. Staikov, and W. Lorenz, Electrochimica Acta **40**, 1385 (1995).

[50] K. Böer, *Survey of Semiconductor Physics* (Van Nostrand Rienhold, New York, 1990).

[51] B. Berghoff, S. Suckow, R. Rolver, B. Spangenberg, H. Kurz, A. Sologubenko, and J. Mayer, J. Appl. Phys. **106**, 083706 (2009).

[52] V. Osinniy, S. Lysgaard, V. Kolkovsky, V. Pankratov, and A. N. Larsen, Nanotechnology **20**, 195201 (2009).

[53] F. Ortmann, F. Bechstedt, and K. Hannewald, Phys. Rev. B **79**, 235206 (2009).

[54] R. A. Marcus, Rev. Mod. Phys. **65**, 599 (1993).

[55] L. Brus, Phys. Rev. B **53**, 4649 (1996).

[56] J. Martin, F. Cichos, F. Huisken, and C. von Borczyskowski, Nano Lett. **8**, 656 (2008).

[57] H. B. Gray and J. R. Winkler, Proc. Nat. Acad. Sci. **102**, 3534 (2005).